

Invited Research Article

A dynamic ocean driven by changes in CO₂ and Antarctic ice-sheet in the middle MioceneAmanda Frigola^{*}, Matthias Prange, Michael Schulz

MARUM – Center for Marine Environmental Sciences, University of Bremen, 28359 Bremen, Germany



ARTICLE INFO

Editor: Dr. Paul Hesse

Keywords:

Modelling
Deep water formation
Ice-sheet
CO₂
Miocene

ABSTRACT

The middle Miocene climate transition (MMCT), likely triggered by a decrease in atmospheric CO₂ concentration and changes in the Earth's orbital configuration, entailed major expansion of the Antarctic ice-sheet and cooling of the global ocean at ~15–13 Ma. By comparing simulations that use boundary conditions representative of 15 and 13 Ma, we assess the response of ocean temperatures and deep ocean circulation to atmospheric CO₂ drawdown (from 400 to 200 ppmv) and Antarctic ice-sheet expansion (43 m of sea-level equivalent) during the MMCT by means of the Community Climate System Model version 3. The model simulates a decrease in mean global sea-surface temperature by 1.6 °C across the transition. Individual forcing experiments reveal that surface cooling is fully attributable to the CO₂ drop, whereas expansion of the Antarctic ice-sheet tends to cause a slight global warming of the upper ocean. At depth, modelled ocean temperatures decrease by 1.5–2 °C across the MMCT in most regions. While the CO₂ effect dominates deep-ocean cooling, about 25–30% is attributable to the expansion of the Antarctic ice-sheet.

In the convection regions of the Southern Ocean, the CO₂ drawdown causes an increase in salinity through sea ice formation and changes in the precipitation-evaporation balance. This increase in salinity, together with a decrease in surface temperatures, translates into an intensification in Antarctic Bottom Water formation that cools the deep ocean. The contribution of the Antarctic ice-sheet expansion to bottom and deep water cooling occurs through an increase in the surface heat flux from the ocean to the atmosphere, which is linked to intensified cold surface winds blowing off the Antarctic continent.

This study suggests that the magnitude of cooling of deep waters across the MMCT inferred from proxy records can be explained by the combined effects of the CO₂ decrease and Antarctic ice-sheet expansion. Our surface cooling estimates are generally lower than those indicated by proxies.

1. Introduction

The middle Miocene climate transition (MMCT; ~ 14.8–13.5 Ma), preceded by a period of global warmth, the middle Miocene climatic optimum (MMCO; ~ 17–14.8 Ma), was a major cooling step in the Cenozoic, involving expansion of the Antarctic ice-sheet, cooling of the surface and deep ocean, and substantial global sea-level fall (Woodruff and Savin, 1991; Flower and Kennett, 1993, 1994, 1995; Lear et al., 2000, 2010; Shevenell et al., 2004, 2008; Holbourn et al., 2005; John et al., 2011). Benthic δ¹⁸O records document an increase of ~0.8–1.2‰ across the transition (Lear et al., 2010; Shevenell et al., 2008), with the main isotopic step occurring at 13.9–13.8 Ma (Holbourn et al., 2014; Lear et al., 2015) (Mi-3 event) and 65–70% of it reflecting Antarctic ice sheet expansion (Shevenell et al., 2008). Ice expansion is also reflected

in the sea level record. Backstripping studies indicate an important eustatic sea level fall across the MMCT, ~20 m between ~14.2 and 12.8 Ma according to Kominz et al. (2008) or 53–69 m between 16.5 and 13.9 Ma according to John et al. (2011). Data from the ANDRILL-2A (AND-2A) site, in the western Ross Sea, 30 km off the coast of Southern Victoria Land, shows evidence of local marine ice sheet advance during the MMCT at 13.8 and 14.6 Ma (Levy et al., 2016). That record indicates that during the MMCO, warmth intervals (6 °C sea-surface temperatures, SSTs; upper 200 m) were interposed with cool temperate (3.5 °C SSTs) and cold polar (1.3 °C SSTs) intervals, meaning that a high climate variability characterized also the MMCO. High-amplitude climate variability prior to the transition is further confirmed by benthic δ¹⁸O records. Holbourn et al. (2014) describe fluctuations in the δ¹⁸O record between 1.9‰ and 0.7‰ within the interval 15.7–14.7 Ma. Deep water

^{*} Corresponding author.

E-mail address: afrigolaboix@gmail.com (A. Frigola).

<https://doi.org/10.1016/j.palaeo.2021.110591>

Received 24 September 2020; Received in revised form 21 July 2021; Accepted 26 July 2021

Available online 30 July 2021

0031-0182/© 2021 Elsevier B.V. All rights reserved.

temperatures (DWTs) exhibit moderate variability across the MMCO and the MMCT (1–3 °C decrease across the transition), as inferred from Mg/Ca (Lear et al., 2000, 2010, 2015; Billups and Schrag, 2002) and clumped isotope-based studies (Modestou et al., 2020). SSTs show a much higher variability than DWTs both across the MMCO and MMCT (range between 0.7 and ≥ 8 °C) and a mean decrease of approximately 3 °C across the transition (Super et al., 2018, 2020; Zhang et al., 2013; Rousselle et al., 2013; Kuhnert et al., 2009; Shevenell et al., 2004; Leutert et al., 2020; Sangiorgi et al., 2018; Levy et al., 2016).

The study of Miocene climate changes and their mechanisms may help improve our understanding of how global temperatures and ocean circulation respond to changes in greenhouse gas concentrations and ice-sheet volumes. Therefore, the MMCT provides an interesting potential “reversed” analogy of modern climate change.

Suggested driving mechanisms for the MMCT include a drop in atmospheric CO₂, changes in ocean circulation and water-mass distribution driven by changing ocean gateways, and orbitally triggered changes in atmospheric energy and moisture fluxes (Flower and Kennett, 1994; Holbourn et al., 2005, 2007). Based on stable isotope records from ODP Sites 1146 and 1237, Holbourn et al. (2005) suggested changes in the Earth’s orbital configuration along with atmospheric CO₂ concentrations as the main triggers of the MMCT. At IODP Site U1338, a switch in the benthic $\delta^{18}\text{O}$ beat from eccentricity- to obliquity-paced is observed at the onset of the MMCT (Holbourn et al., 2014). Data from the AND-2A drill site point to a correlation between CO₂ variations and local expansion of the Antarctic ice-sheet across the MMCT (Levy et al., 2016). Using an isotope-enabled ice sheet–climate model forced with a decrease in atmospheric CO₂ and time-varying orbital parameters, Langebroek et al. (2010) simulated an increase in seawater $\delta^{18}\text{O}$ in good agreement with published isotope records from the MMCT. Gasson et al. (2016) showed that changes in atmospheric CO₂, consistent with reconstructed values, along with variations in the Earth’s orbital configuration, can explain the variability of the Antarctic ice-sheet volume during the MMCT as inferred from $\delta^{18}\text{O}$ and sea-level studies.

Even though the exact causes and mechanisms of the MMCT are still a matter of debate, the studies cited above are indicative that a drop in atmospheric CO₂ and an expansion of the Antarctic ice-sheet were involved, either as a trigger or a feedback. So far, the literature for MMCT global atmosphere–ocean simulations is limited to one study by Knorr and Lohmann (2014). Analogously to Knorr and Lohmann (2014), the focus of the current study is to analyze the individual and combined effects of atmospheric CO₂ drawdown and Antarctic ice-sheet expansion on the cooling of the ocean. Knorr and Lohmann (2014) model a decrease in surface air temperature of 3.1 °C as a response to the CO₂ and ice-sheet forcings, increased deep water convection in the Southern Ocean caused on one side by CO₂-induced surface cooling, and to a lesser extent, by local sea-ice changes linked to topography-related modified winds around Antarctica. Our study employs a different model and boundary conditions, and it has a different perspective since it emphasizes on deep water mass properties and circulation aspects, in both southern and northern high latitudes.

Here we address the following specific questions by means of climate model experiments using the global coupled Community Climate System Model version 3 (CCSM3): Can the combined effects of the middle Miocene CO₂ decrease and Antarctic ice-sheet expansion explain the magnitude of cooling of surface and deep waters across the MMCT inferred from proxy data? What are the separate effects of these two forcings on surface and deep-water temperatures? What mechanisms stand behind ocean cooling? What changes are observed in water mass properties and circulation at high latitudes?

2. Methods

2.1. Model and experimental design

Model simulations were performed with CCSM3, a fully coupled

general circulation model consisting of components representing atmosphere, ocean, land, and sea ice (Collins et al., 2006). We used a T42 (~2.8° resolution) grid for the atmosphere and land components in combination with a 384 × 320 grid for the ocean and sea-ice components. The atmosphere and ocean vertical grids have 26 and 40 levels, respectively (see Frigola et al., 2018, for further details).

Four middle Miocene sensitivity experiments named MMCO400 (equivalent to experiment MMCO of Frigola et al., 2018), MMCO200, MMG400, and MMG200 (equivalent to experiment MMG of Frigola et al., 2018), plus a pre-industrial (PI) control experiment were carried out. All Miocene experiments use middle Miocene global topography, bathymetry and vegetation (Table 1). The experimental designs of the four Miocene experiments differ in terms of Antarctic ice-sheet volume, sea level, and atmospheric CO₂ concentration.

In MMCO400, atmospheric CO₂ concentration is set to 400 ppmv and Antarctic ice-sheet volume to 6 million km³ (retreated ice-sheet). In MMG200, atmospheric CO₂ concentration is set to 200 ppmv and Antarctic ice-sheet volume to 23 million km³ (expanded ice-sheet). Despite uncertainties in the boundary conditions, values employed in the MMCO400 and MMG200 experiments are within the range of published estimates for the periods before (~15 Ma) and after (~13 Ma) the MMCT, respectively (Frigola et al., 2018). Comparison of the MMCO400 and MMG200 experiments (MMG200 minus MMCO400) would thus show climatic changes across the MMCT.

In the MMCO200 experiment, all boundary conditions are kept the same as in MMCO400, except for CO₂, which is lowered to 200 ppmv. The MMG400 experiment has a design identical to that of MMG200, except for CO₂, which is set to 400 ppmv. Experiments MMCO200 and MMG400 are aimed at disentangling the effect of the Antarctic ice-sheet expansion from that of the CO₂ decrease across the MMCT.

In the PI experiment, well-mixed greenhouse gases, ozone distribution, aerosols, solar constant and orbital configuration are set to PI following Otto-Bliesner et al. (2006). In the Miocene experiments, these same settings are used, except for atmospheric CO₂ values (Table 2).

Compared to the previous study by Knorr and Lohmann (2014), our atmospheric CO₂ concentration values are lower (400 and 200 ppmv vs. 450 and 278 ppmv). Regarding Antarctic ice-sheet dimensions, Knorr and Lohmann (2014) use a volume four times smaller than the present-day value for the small ice-sheet configuration (similar to our 6 million km³ value, assuming a present-day Antarctic ice volume of 27 million km³; Fretwell et al., 2013) and a present-day value for the large ice-sheet configuration (which is bigger than our 23 million km³ value). In that study surface albedo is kept constant, in contrast to the current setup. Orbital configuration is set to present-day values.

The PI experiment was branched from the NCAR CCSM3 1870 CE control run and integrated for another 150 years (i.e., 850 years in total). The Miocene experiments were integrated for a total of 1500 years each. The last 100 years of each simulation were used for the analyses. The temperature trends in the deep ocean (4–5 km depth) were < 0.14, 0.15, 0.17, 0.185, and 0.13 °C/100 years in the PI, MMCO400, MMG200, MMCO200, and MMG400 cases, respectively. At that same depth range, the salinity trends were < 0.01, 0.007, 0.01, 0.014, and 0.025 g/kg/100 years for PI, MMCO400, MMG200, MMCO200, and MMG400, respectively. Although only quasi-equilibrium states were reached, tendencies are small enough to allow for a robust interpretation of the model results. Unless otherwise specified, figures show annual means of climatic variables.

2.2. Uncertainties in boundary conditions

Middle Miocene Antarctic ice volume estimates for the MMCT available from the literature are obtained through indirect methods (sea level, $\delta^{18}\text{O}_{\text{sw}}$ or modelling studies). Our values of 6 million km³ for a retreated ice-sheet, and 23 million km³ for an expanded ice-sheet, are based on Langebroek et al. (2009) and Oerlemans (2004) modelling studies and thus lie within the range of published estimates (see section

Table 1Summary of Antarctic ice-sheet volume, sea level, CO₂, topography/bathymetry, and vegetation for the middle Miocene experiments.

	MMCO400	MMG200	MMCO200	MMG400
Atmospheric CO ₂ Concentration	400 ppmv	200 ppmv	200 ppmv	400 ppmv
Antarctic Ice-Sheet Volume	6 million km ³	23 million km ³	same as MMCO400	same as MMG200
Sea level	48 m higher than at present-day	5 m higher than at present-day		
Global Topography/Bathymetry	mainly Herold et al. (2008) with modifications for tropical seaways (Hall, 2012 ; Montes et al., 2012) and the Antarctic ice-sheet	same as MMCO400, but with global sea level reduced by 43 m and an expanded Antarctic ice-sheet		
Global Vegetation	mainly Pound et al. (2012) with gaps filled according to Wolfe (1985) and Morley (2011) ; ice and tundra in Antarctica	same as MMCO400, but with tundra removed in Antarctica		

Table 2

Summary of atmospheric composition, solar constant, and orbital configuration for the CCSM3 experiments.

Experiment	PI	MMCO400	MMG200	MMCO200	MMG400
CO ₂	280 ppmv	400 ppmv	200 ppmv	200 ppmv	400 ppmv
CH ₄	760 ppbv	same as PI			
N ₂ O	270 ppbv				
CFC's	0				
O ₃	1870 A. D.				
Sulfate Aerosols	1870 A. D.				
Dust and Sea Salt	PD				
Carbonaceous Aerosols	30% of PD				
Solar Constant	1365 W m ⁻²				
Eccentricity	0.016724				
Obliquity	23.446 °				
Precession	102.04 °				

Note: PI values are according to [Otto-Bliesner et al. \(2006\)](#). The orbital configuration represents 1950 AD values. PD denotes present-day.

2 in [Frigola et al., 2018](#)). These ice volumes are consistent with published estimates of sea level change across the MMCT (see section 3 in [Frigola et al., 2018](#)). A more recent modelling study providing Antarctic ice volume estimates for the MMCT is that of [Gasson et al. \(2016\)](#). Two different approaches are adopted in that study. The first one assumes a present-day bedrock topography (scenario A); the second one scales an earlier Eocene–Oligocene topography ([Wilson et al., 2012](#)) assuming constant rates of Antarctic topography change from 34 Ma to present-day (scenario B). In scenario A, an increase in ice volume of 15.2–17.9 million km³, from 8.8–11.5 to 26.7 million km³ is modelled. Our amplitude of change (17 million km³) is in good agreement with that scenario, although our absolute values are slightly lower. In scenario B, an increase in ice volume of 18.3–21.4 million km³, from 14.1–17.2 million km³ to 35.5 million km³ is modelled. These values are higher compared to our study. However, ice volume depends on bedrock topography and the latter presents uncertainties. A stronger ocean response would be expected with higher ice volume variability. Quantification of ocean response variability associated with ice volume uncertainties is important and should be addressed in future studies. Uncertainties in middle Miocene CO₂ estimates are very high, with a wide range of reconstructed values ([Raitzsch et al., 2021](#); [Steinthsordottir et al., 2021](#)). Nevertheless, the most recent reconstructions suggest CO₂ values of 400–600 ppmv during the MMCO and a decrease in CO₂ across the MMCT (section 8 and Fig. 5 in [Steinthsordottir et al., 2021](#)). Our value of 400 ppmv coincides with the lower limit for the MMCO interval. Employment of higher CO₂ values in the experiment set

up would lead to higher modelled temperatures. For further details on the choice of our CO₂ values the reader is referred to section 4 of [Frigola et al. \(2018\)](#).

As mentioned above, a PI orbital configuration is used in the current study. Orbital changes played a role in climate variability during the middle Miocene ([Holbourn et al., 2014](#)). [Burls et al. \(2021\)](#) (subsection 4.2 and Fig. 8 in that study) suggest important though relatively small (compared to other boundary conditions) surface temperature sensitivity to orbital changes. In view of this evidence, additional sensitivity experiments testing warm and cold orbits would constitute a valuable goal for future studies.

3. Results

3.1. Middle Miocene versus pre-industrial ocean states

Our experiments indicate a middle Miocene climate warmer than PI with global mean 2-m surface air temperatures 4.22 °C and 1.72 °C higher for MMCO400 and MMG200, respectively. Modelled global mean SSTs are 2.77 and 1.19 °C warmer for MMCO400 and MMG200, respectively ([Fig. 1](#)). The oceanic regions showing the strongest anomalies compared to PI are the northern North Pacific, where MMCO400 SSTs are more than 4 °C warmer than PI, the North Atlantic, as well as a circumpolar belt south of 40° S ([Fig. 1](#)). Middle Miocene global mean ocean temperatures at depth are warmer than PI as well: 2.72 °C and 1.1 °C higher at 2000–2250 m for MMCO400 and MMG200, respectively. The strongest warming occurs in the high northern latitudes. In the MMCO400 (MMG200) experiment, at that depth interval, temperatures are 4–5 °C (2–3 °C) higher in the North Atlantic and 9–10 °C (7–8 °C) higher in the Arctic Ocean (not shown). A noticeable result in the middle Miocene experiments is the weaker Antarctic Circumpolar Current (ACC) compared to PI ([Fig. S6](#)). At the Drake Passage, for example, the intensity of the ACC is about 130 Sv for the MMCO400 versus 190 Sv for PI. Another feature is the stronger deeper and the weaker upper cells of the meridional overturning circulation (MOC) in the Miocene experiments compared to PI associated with changes in the formation rates of Antarctic Bottom Water (AABW) and North Atlantic Deep Water (NADW), respectively ([Fig. 2](#)). Besides, the middle Miocene experiments exhibit increased southward ocean heat transport in the Southern Hemisphere (up to 0.7 PW more at ~12°S for MMCO400) and decreased northward ocean heat transport in the Northern Hemisphere (up to 0.35 PW less at ~15°N for MMCO400; not shown).

3.2. Changes in sea-surface temperatures across the MMCT

Mean global SST decreases from 19.6 °C at MMCO400 to 18.0 °C at MMG200. The regions showing the most pronounced cooling are the northern North Pacific (2–5 °C) and some areas of the Southern Ocean (up to ~5 °C of cooling) ([Fig. 3a](#)). The effect of the atmospheric CO₂ decrease on SST can be analyzed by comparing experiment MMCO200

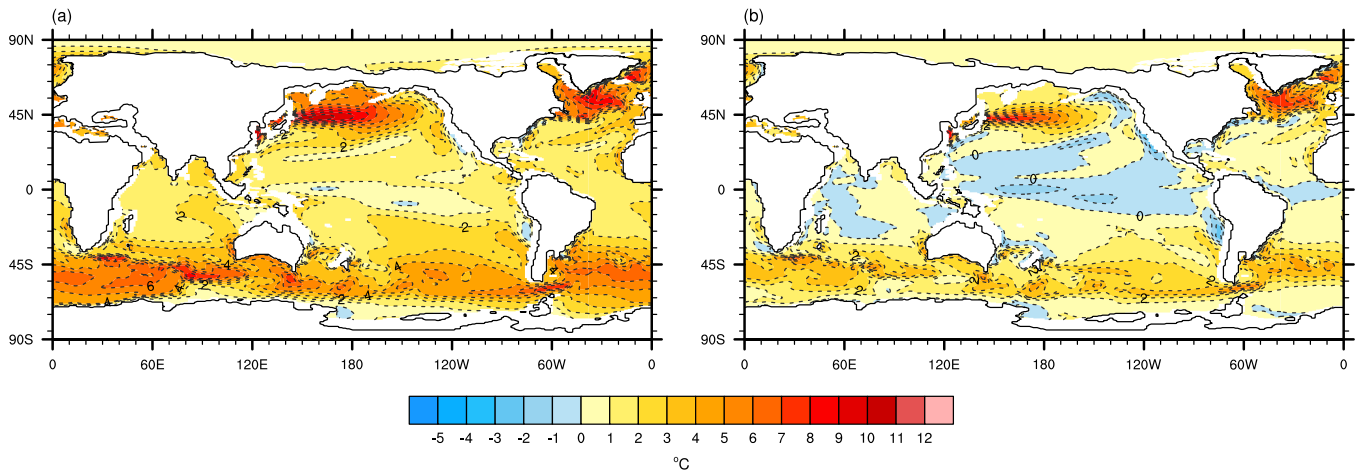


Fig. 1. Mean annual sea-surface temperature differences: a) MMCO400-PI, and b) MMG200-PI, in °C. Note: these data correspond to Fig. 6 b) in Frigola et al. (2018). Black lines indicate the middle Miocene coastline. Non-coloured regions represent either middle Miocene or present-day land areas.

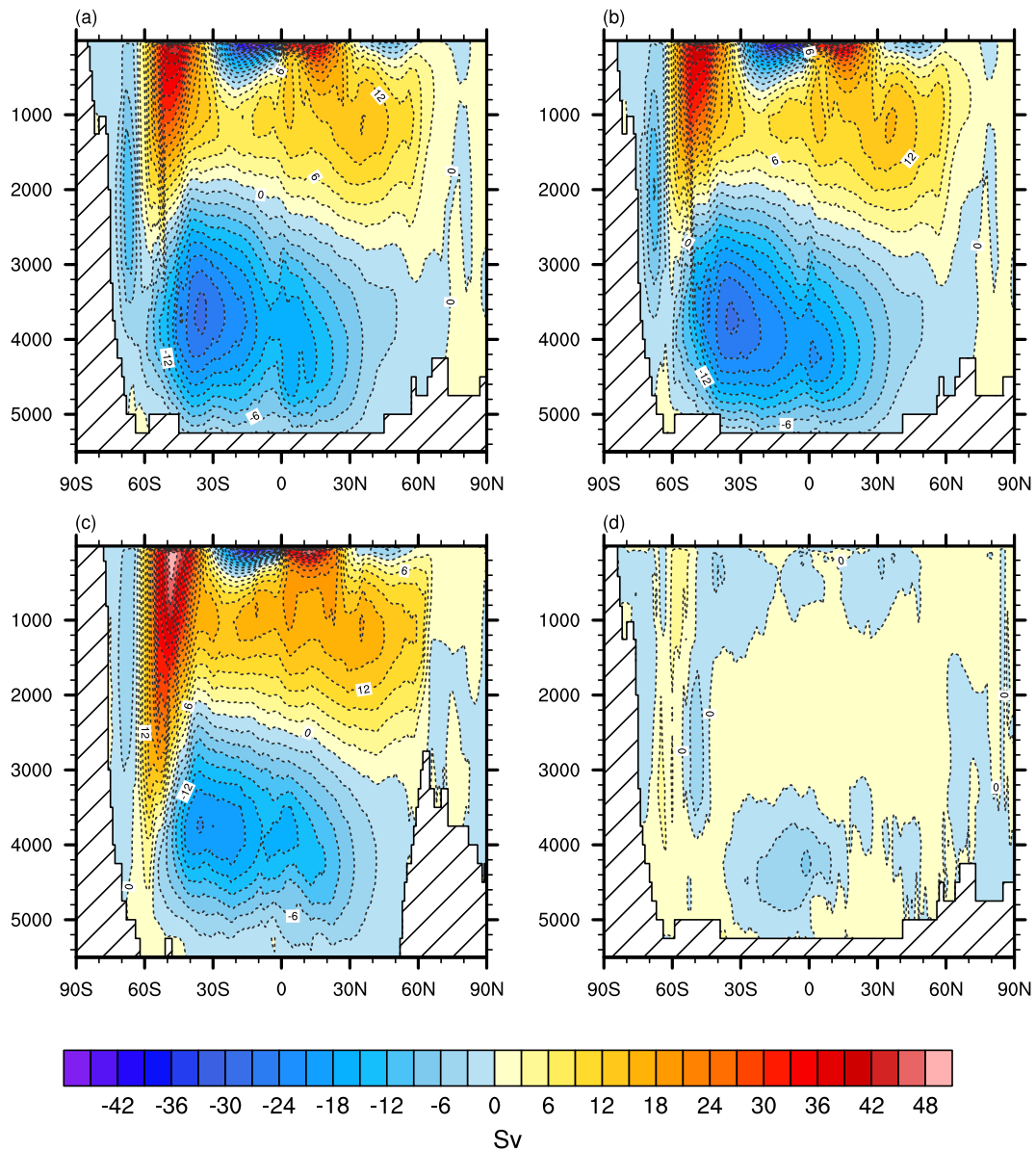


Fig. 2. Global meridional overturning circulation (MOC) streamfunction (Eulerian component): a) MMCO400, b) MMG200, c) PI, and d) MMG200-MMCO400, in Sv.

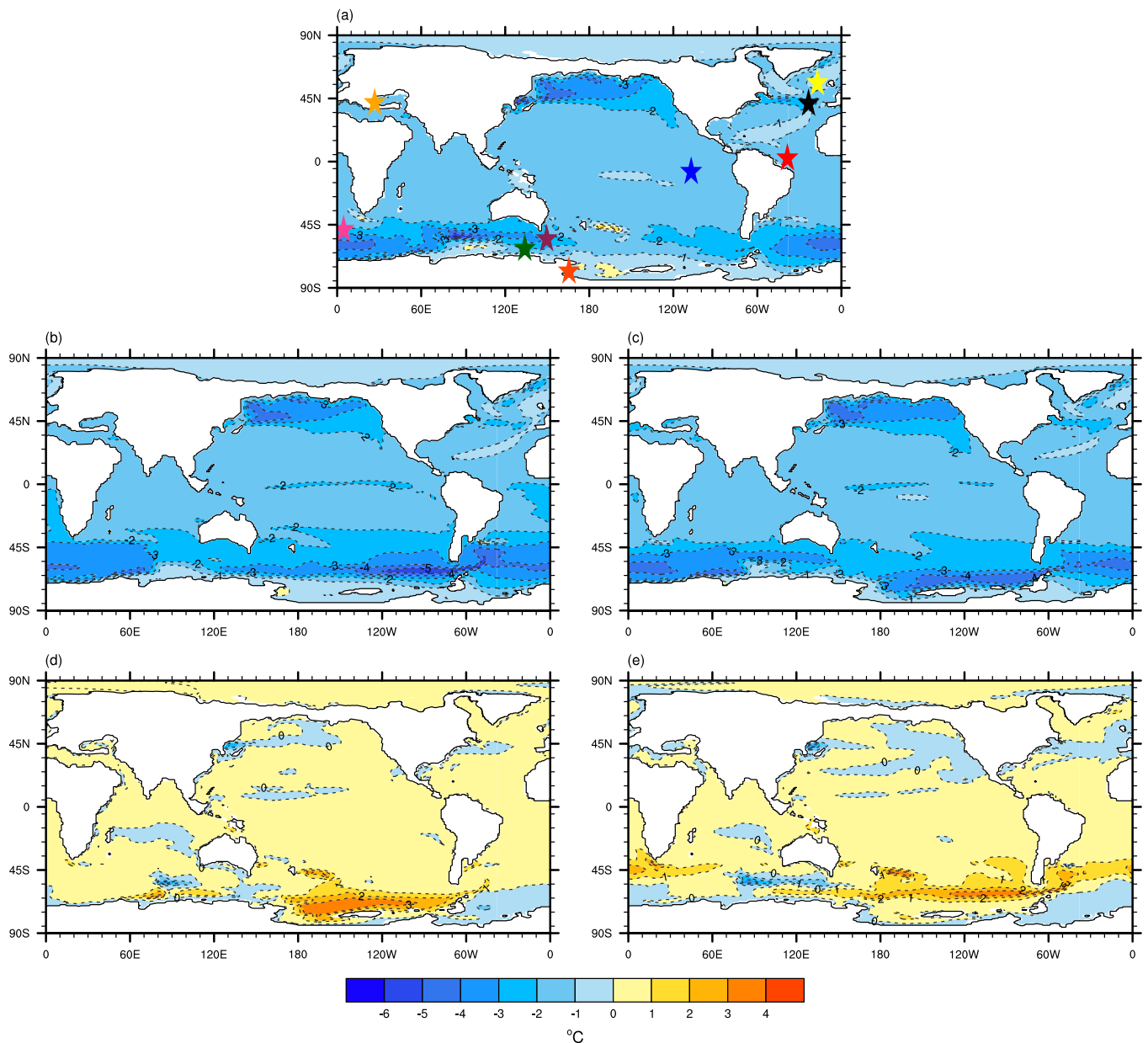


Fig. 3. Mean annual sea-surface temperature differences: a) MMG200-MMCO400 (MMCT), b) MMCO200-MMCO400 and c) MMG200-MMG400 (CO₂ effect), and d) MMG400-MMCO400 and e) MMG200-MMCO200 (ice-sheet effect), in °C. Stars show middle Miocene datashites: ODP 982 (yellow); LOM-1 (light orange); DSDP 608 (black); ODP 925 (red); IODP U1338 (blue); ODP 1092 (light violet); ODP1171 (dark violet); IODP U1356 (green); AND-2A (dark orange). (For interpretation of the references to colour in this figure legend, the reader is referred to the web version of this article.)

against MMCO400 (retreated ice-sheet) and experiment MMG200 against MMG400 (expanded ice-sheet). A significant decrease in mean global SST is observed in both cases: 2.0 °C with a retreated Antarctic ice-sheet, and 1.9 °C with an expanded Antarctic ice-sheet. Again, cooling is most pronounced in the Southern Ocean and in the northern North Pacific (Fig. 3b,c). By comparing experiment MMG400 against MMCO400 and MMG200 against MMCO200, the effect of the Antarctic ice-sheet expansion is assessed. In both cases slight increases in mean global SST are observed: 0.3 °C with CO₂ fixed at 400 ppmv, and 0.4 °C with CO₂ fixed at 200 ppmv. Warming is particularly pronounced in some regions of the Southern Ocean, with increases in temperature by up to 3 °C (Fig. 3d, e). Although warming is the dominant trend, a few localized cooling patterns are also detected in the simulations, e.g. in the Southern Ocean and the Northwest Pacific. Globally, the effects of CO₂ and Antarctic ice-sheet on SST are opposite in sign and the effects of the first dominate over those of the latter.

3.3. Changes in deep and bottom-water temperatures across the MMCT

Waters cool down across the MMCT (MMG200 minus MMCO400) at almost all depths and latitudes (Fig. 4a). In most regions, ocean temperatures decrease by 1.5–2 °C. The CO₂ decrease alone (MMCO200 minus MMCO400 and MMG200 minus MMG400) causes significant cooling of waters at almost all depths and latitudes (Fig. 4b, c). However, this cooling effect is weaker in the lower cell of the MOC compared to the upper cell. The effect of the Antarctic ice-sheet expansion (MMG400 minus MMCO400 and MMG200 minus MMCO200) on ocean temperatures is not uniform and varies significantly with depth (Fig. 4d, e). Cooling dominates at depths below ~1400 m, while warming occurs above this level (and also at deeper levels in the Arctic for the MMG200 minus MMCO200 case). The zonal-mean temperature distribution indicates that the Antarctic ice-sheet expansion cools down waters close to the surface at high southern latitudes and that these waters spread to

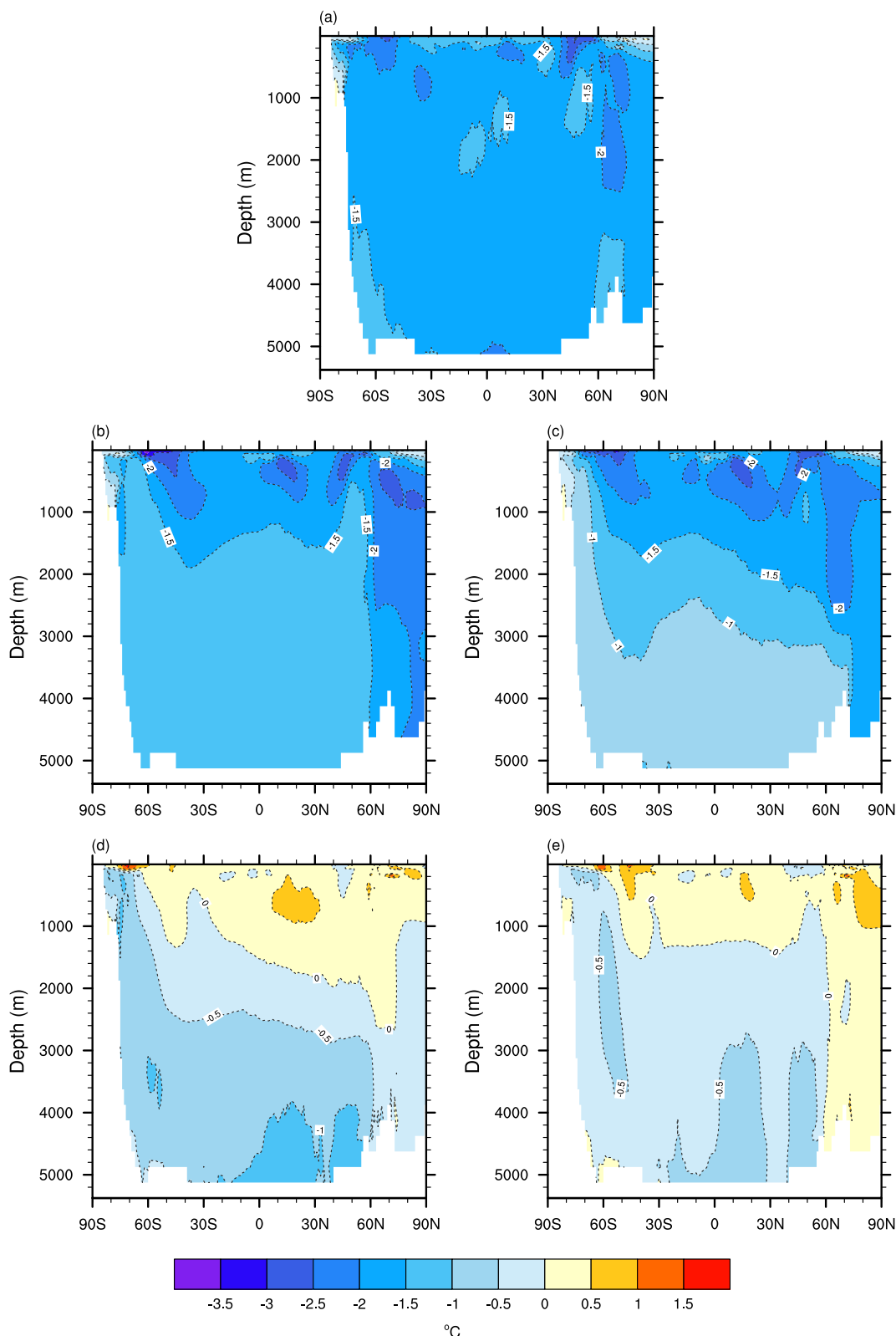


Fig. 4. Zonally averaged temperature differences: a) MMG200-MMCO400 (MMCT), b) MMCO200-MMCO400 and c) MMG200-MMG400 (CO₂ effect), and d) MMG400-MMCO400 and e) MMG200-MMCO200 (ice-sheet effect), in °C.

lower latitudes through the lower cell of the MOC (Fig. 4d, e). Both the CO₂ decrease and the Antarctic ice-sheet expansion contribute to cooling of the deep ocean across the MMCT, although the CO₂ cooling effect is generally stronger. In order to identify the areas where upper-ocean cooling is transmitted to the deep ocean, temperature changes at

2000–2250 m depth are plotted (Fig. 5). At this depth interval, global mean temperatures decrease from 3.6 °C at MMCO400 to 2.0 °C at MMG200. The strongest cooling is simulated in an area of the Southern Ocean between ~80–160° E, south of Australia, where temperatures decrease by 2.5–3 °C, and in the North Atlantic, where temperatures

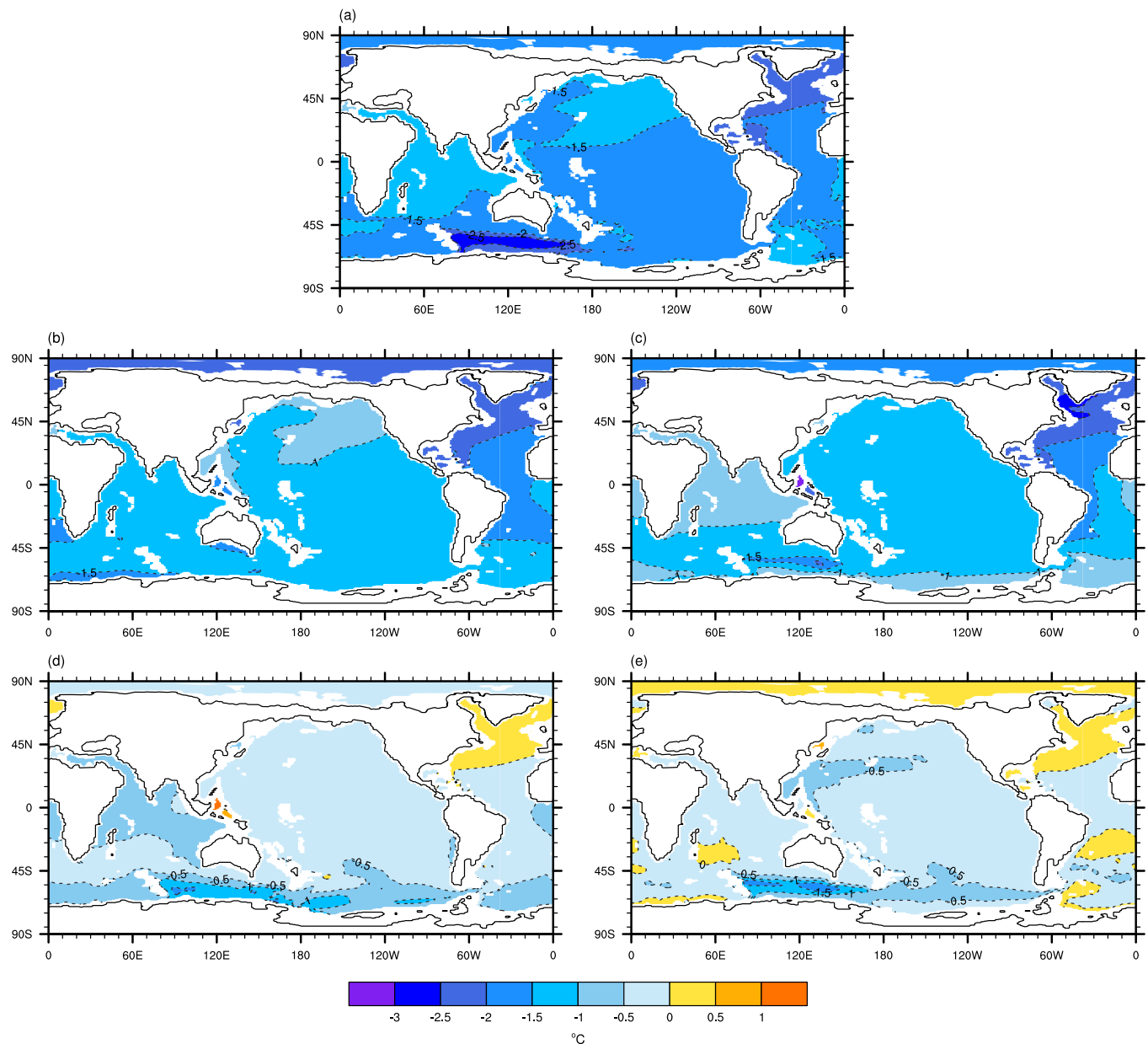


Fig. 5. Deep-ocean temperature differences at 2000–2250 m depth: a) MMG200-MMCO400 (MMCT), b) MMCO200-MMCO400 and c) MMG200-MMG400 (CO_2 effect), and d) MMG400-MMCO400 and e) MMG200-MMCO200 (ice-sheet effect), in $^{\circ}\text{C}$.

decrease by up to 2–2.5 $^{\circ}\text{C}$ (Fig. 5a). These results indicate that cooling of deep waters in the Southern Ocean is caused both by the CO_2 decrease and the Antarctic ice-sheet expansion, while cooling in the deep North Atlantic is caused exclusively by the CO_2 decrease (Fig. 5b–e).

3.4. Deep ocean circulation changes in the Southern Ocean during the MMCT

Across the MMCT, Southern Ocean waters cool by 1.5–2 $^{\circ}\text{C}$ at depth and salinities increase by about 0.1 g/kg (Fig. 6a), leading to an increase in potential density of about 0.2–0.25 kg/m^3 (not shown). While cooling of the Southern Ocean is related to both the Antarctic ice-sheet and the CO_2 forcings, the increase in deep- and bottom-water salinities can be attributed exclusively to the atmospheric CO_2 decline (Fig. 6b–e). A closer inspection of Southern Ocean surface freshwater fluxes indicates that the CO_2 -induced salinity increase is caused by freshwater/salt flux anomalies linked to increased sea-ice formation around the Antarctic continent (Fig. 7) in combination with a reduction in precipitation-

minus-evaporation due to a weaker hydrologic cycle in the colder atmosphere (Fig. 8). The temperature- and salinity-induced increase in AABW density causes slight strengthening of the lower MOC cell (~ 6 Sv at the equator) in MMG200 compared to MMCO400 (Fig. 2).

3.5. North Atlantic deep water formation during the middle Miocene

The patterns of winter mixed layer depth reveal the regions of convection and deep water formation in the North Atlantic at MMCO400 and MMG200 (Fig. 9). Compared to MMCO400 the mixed layer deepens in MMG200 southeast of Greenland. The same happens in experiment MMCO200 (Fig. 9c) indicating that the CO_2 drop is responsible for intensified convection and a deeper mixed layer. As a result, a moderate strengthening of the upper (NADW-related) MOC cell across the MMCT is observed of about ~ 1 Sv (Fig. 2). Increased convective activity in the North Atlantic in response to declining CO_2 is related to an increase in the surface heat flux from the ocean to the atmosphere (Fig. S8). In all Miocene experiments, however, NADW-equivalent water masses are

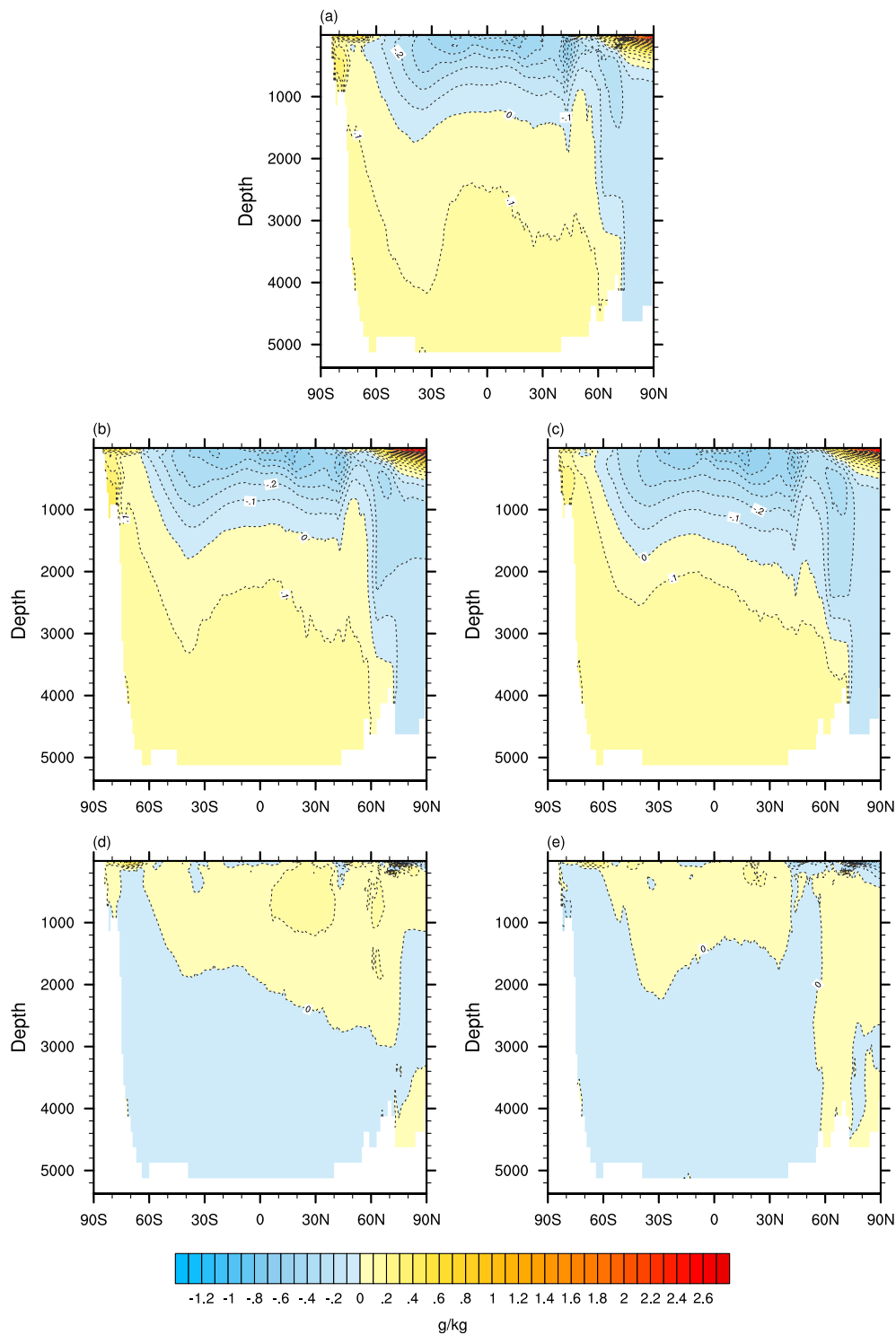


Fig. 6. Zonally averaged salinity differences: a) MMG200-MMCO400 (MMCT), b) MMCO200-MMCO400 and c) MMG200-MMG400 (CO₂ effect), and d) MMG400-MMCO400 and e) MMG200-MMCO200 (ice-sheet effect), in g/kg.

characterized by relatively high salinities (Fig. 10), indicating that salinity plays a key role in middle Miocene deep water formation.

3.6. Antarctic ice-sheet effects on global surface and deep-water temperatures

Opposite effects of the Antarctic ice-sheet expansion on upper and deep-ocean temperatures were found: while mean temperature increases in the upper ocean, AABW equivalent water cools down and

mixes with deep waters. Our results, thus, are in agreement with Knorr and Lohmann (2014), whose model experiments show a similar feature.

In our experiments, global upper ocean warming arises from the increase in Antarctic elevation (see Frigola et al., 2018), which affects the atmospheric energy balance through a change in the longwave radiation. Surface cooling over Antarctica induced by the increased topography (Fig. S1) causes a decrease in the outgoing longwave flux at the top of the atmosphere (Fig. S2), inducing a reduction in the southward atmospheric energy transport towards the Antarctic and thus a

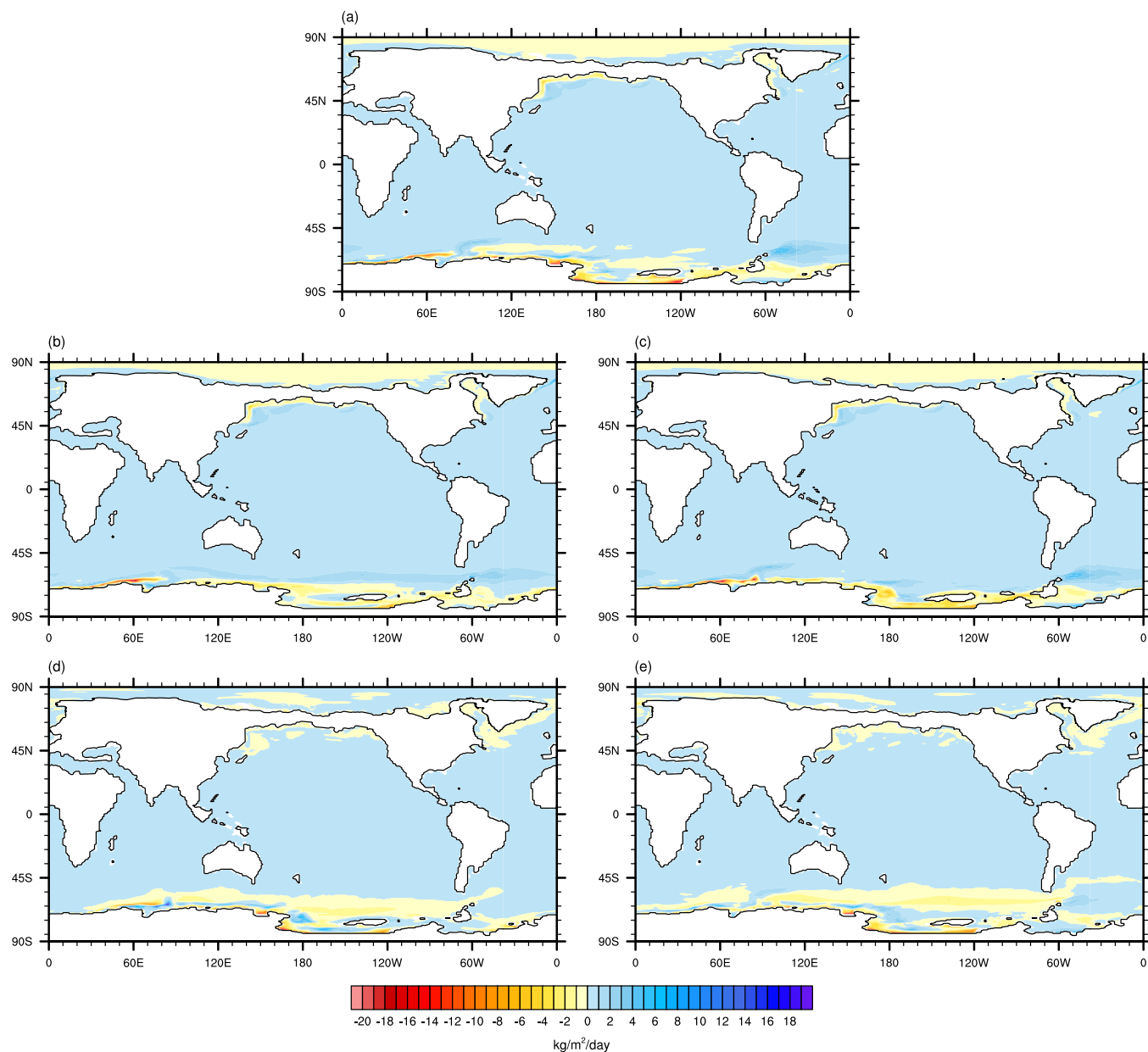


Fig. 7. Surface freshwater-flux differences related to sea-ice formation and melting: a) MMG200-MMCO400 (MMCT), b) MMCO200-MMCO400 and c) MMG200-MMG400 (CO_2 effect), and d) MMG400-MMCO400 and e) MMG200-MMCO200 (ice-sheet effect), in kg of freshwater/ m^2/day . Positive values indicate an increase in freshwater into the ocean.

general increase in air temperatures and, via air-sea heat fluxes, SSTs outside Antarctica (Singh et al., 2016). Also deep water cooling induced by the Antarctic ice-sheet expansion is linked to the increased topography. A higher elevation of the East Antarctic Ice Sheet leads to an increase in the pressure gradient between the polar highs and subpolar lows, which causes stronger cold surface winds blowing off the Antarctic continent (Fig. 11). As a result, surface heat fluxes from the ocean to the atmosphere increase in the Southern Ocean near Antarctic continental margins, in particular south of Australia and in the proto-Ross Sea (90°E – 150°W) (Fig. 11), resulting in cooling of AABW equivalent water that eventually spreads towards north.

4. Discussion

A warmer-than-present middle Miocene climate was simulated, with global surface-air temperatures 4.2 and 1.7 °C higher than PI for MMCO400 and MMG200, respectively, and stronger warming in mid-to-

high-latitudes than in the tropics. A recent study has been published within the Miocene model intercomparison project (MioMIP1) including comparison of modelled vs. proxy-based Miocene surface temperatures (Burls et al., 2021). Data from our simulations are contained in that comparison. Burls et al. (2021) show that currently published GCM simulations do not successfully reproduce the latitudinal surface temperature gradient reconstructed by proxies. Simulations with prescribed low-to-medium CO_2 values (including the submitted study) underestimate middle Miocene high latitude warming, while high CO_2 values simulate too much warmth in the tropics (see Figs. 11, 12 and section 4.3 in Burls et al., 2021) although the latter entail global mean surface temperatures in line with middle Miocene proxy reconstructions (see Fig. 4a and subsection 4.1 in Burls et al., 2021). A clear picture of to what degree our experiments reproduce middle Miocene latitudinal SST patterns is provided in Fig. 12a,b in Burls et al. (2021). A reduction in middle Miocene model boundary conditions and proxy uncertainties, together with improved model physics (Burls et al., 2021), will bring

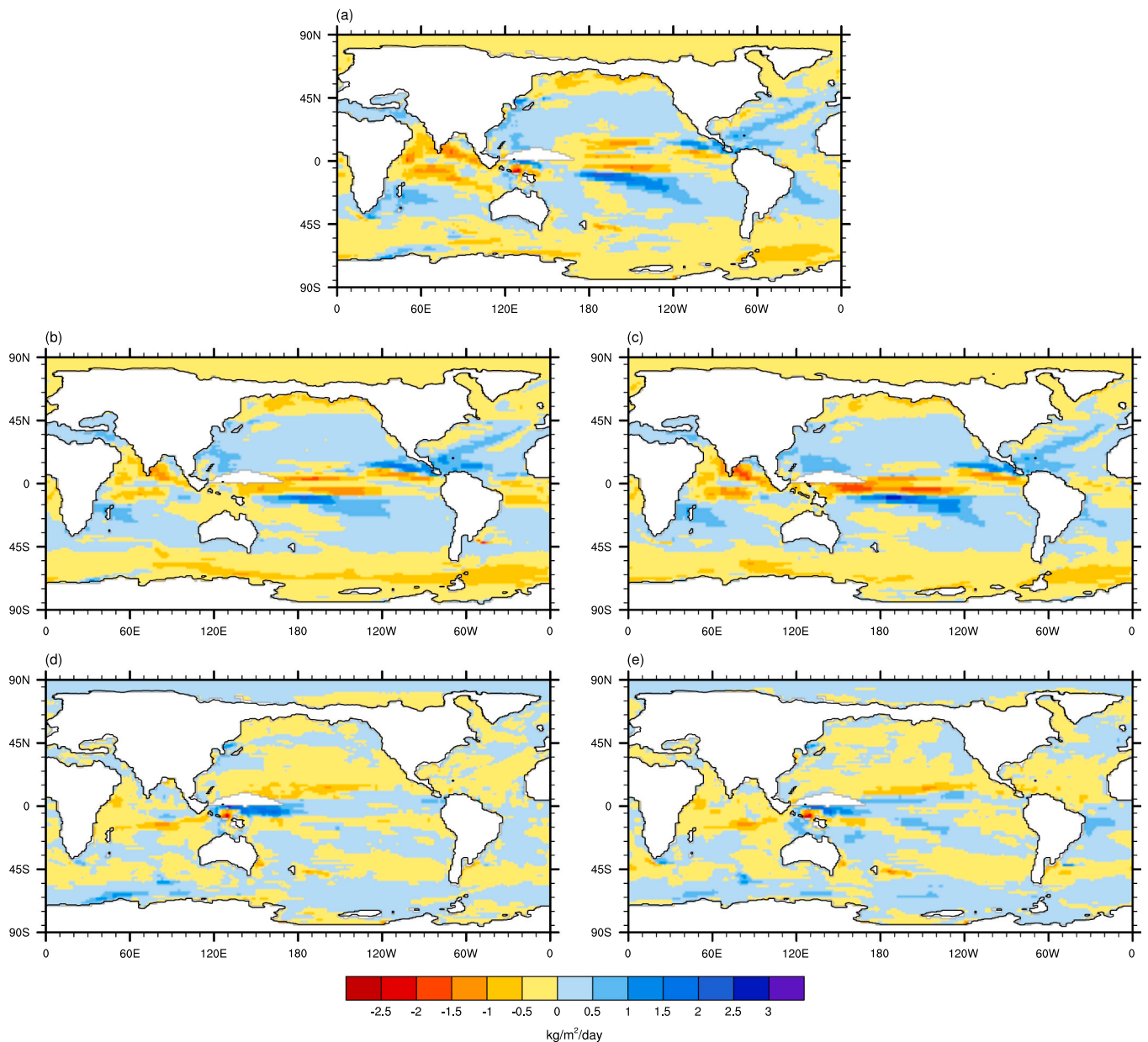


Fig. 8. Surface freshwater-flux differences from precipitation and evaporation: a) MMG200-MMCO400 (MMCT), b) MMCO200-MMCO400 and c) MMG200-MMG400 (CO_2 effect), and d) MMG400-MMCO400 and e) MMG200-MMCO200 (ice-sheet effect), in kg of freshwater/ m^2/day .

model vs. proxy data into better agreement.

In our simulations, warming at MMG200 (compared to PI) occurs despite lower atmospheric CO_2 values, indicating additional factors contribute to middle Miocene warmth (Fig. 1). Topography and specially vegetation and ice-cover changes have been suggested as an important source of warming through reduction of the planetary albedo and a positive water vapor feedback (Knorr et al., 2011). In the MMG200 setup, the lower middle Miocene topography is employed, vegetation includes less dry-adapted biomes, Antarctic ice volume is ~ 4 million km^3 smaller compared to PI and the Greenland ice-sheet is absent (Frigola et al., 2018). All these changes clearly contribute to a lower albedo.

Weakening of the ACC in the Miocene experiments is neither related to a shift of the south westerly winds (Fig. S5) nor to the more southern position of Australia (Fig. S6). Comparison of the SST and barotropic stream function fields indicates a spatial correlation between local sea-surface warming in the Southern Ocean and weakening of the ACC (Fig. 1 and Fig. S6). Our findings are in line with results by Sangiorgi et al. (2018) that suggest either a weaker or displaced ACC during the

MMCO based on a reconstructed reduced latitudinal temperature gradient between ODP Site 1171 (South Tasman Rise) and IODP Site U1356 (Wilkes Land, East Antarctica). Weakening of the ACC is an interesting feature and should be further investigated in future work.

The model simulates a mean global 2-m surface air temperature decrease of 2.5°C along with a mean global SST decrease of approximately 1.6°C across the MMCT, with the most pronounced sea-surface cooling occurring in the Southern Ocean ($2\text{--}4^\circ\text{C}$) and the northern North Pacific ($2\text{--}4^\circ\text{C}$) (Fig. 3). Proxy data indicate surface cooling of $\sim 3^\circ\text{C}$ (range between 0.7 and $\geq 8^\circ\text{C}$) across the MMCT (Table S1) (see Fig. 3a for site locations). Evidence from the northern high latitudes (ODP Site 982) indicates surface cooling of $1.8\text{--}3.7^\circ\text{C}$. Our value for that location is lower, 0.5°C of cooling. Nevertheless, modelled cooling of the sub-surface upper ocean in the North Atlantic is in good agreement with ODP Site 982 estimates (Fig. S3). In the northern mid-latitudes, DSDP Site 608 displays a SST decrease of 6°C , a value significantly higher than our value of 2.3°C for that site. In the tropics, proxy and model estimates come to a better agreement, with our value (1.6°C)

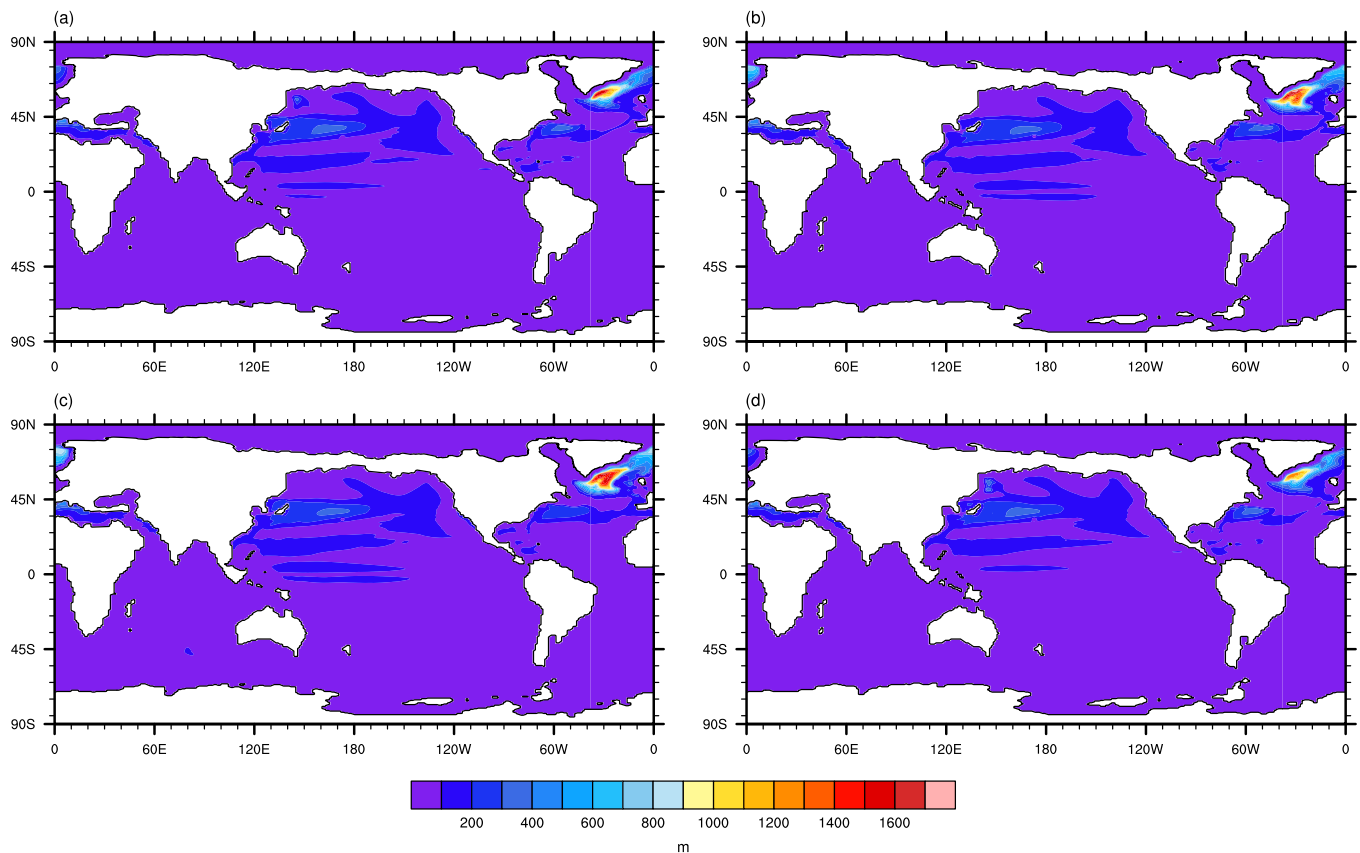


Fig. 9. Boreal winter mean mixed layer depth: a) MMCO400, b) MMG200, c) MMCO200, and d) MMG400, in m.

falling within the range of proxy estimates (0.7–2.6 °C). In the southern mid-latitudes, ODP Site 1092 shows again stronger cooling (6 °C) than the model (1.9 °C). Nevertheless, a bit further south of that site, at ~60°S we modelled a SST drop of ~4 °C, in better agreement with Site 1092 estimate. Meanwhile, ODP Site 1171 and modelled values are in excellent agreement. Finally, sites close to Antarctica, IODP Site U1356 and AND-2A, present the strongest disagreement between model and proxy data, with proxy-inferred cooling ~5 °C stronger than modelled values. We believe the general weaker response in the model might be correlated to the underestimation of Middle Miocene warmth in models previously mentioned. Note the significantly higher absolute SSTs in mid-Miocene proxies compared to the model data (Table S1).

Our results indicate that the forcing responsible for the decrease in mean global SST across the MMCT is the drop in atmospheric CO₂, whereas the elevated Antarctic ice-sheet produces a slight increase in global mean surface temperature as found in previous studies (Knorr and Lohmann, 2014; Singh et al., 2016). In spite of the SST decrease shown in proxy records, this decrease was neither spatially uniform nor synchronized. Besides, although the latest reconstructions show evidence of a CO₂ drawdown across the transition (e.g. Raitzsch et al., 2021), temporal correlation between SSTs and CO₂ does not occur point-to-point (Steinthorsdottir et al., 2021). Our model results confirm that the SST response is region-dependent, with stronger cooling occurring at high latitudes. Ocean heat transport towards high-latitudes increases slightly with the CO₂ decrease (and across the MMCT) (not shown), excluding changes in meridional heat transport as the reason for enhanced high latitude cooling. This implies CO₂ is triggering additional mechanisms at high latitudes, probably through sea-ice changes and local ocean circulation changes, that would explain the asynchronous non-uniform response. In general, the CO₂-temperature-relationship through the Miocene warrants further research and requires a larger database.

We note that the SST response to the two different forcings is highly linear: the global decrease of 1.6 °C in SST across the MMCT is the sum of the SST decrease of 2.0 °C due to the CO₂ decline (retreated ice-sheet) and the SST increase of 0.4 °C due to the Antarctic ice-sheet expansion (CO₂ fixed at 200 ppmv). This finding is qualitatively consistent with earlier results by Knorr and Lohmann (2014), who also assessed the relative roles of CO₂ decrease and Antarctic ice-sheet expansion during the middle Miocene. The global SST warming effect of the Antarctic ice-sheet expansion is related to its increase in elevation.

Our CCSM3 experiments show a decrease in deep-ocean temperatures of 1.5–2 °C at almost all depths and latitudes across the MMCT (Fig. 4). This result is in general agreement with Mg/Ca (Lear et al., 2000, 2010, 2015; Billups and Schrag, 2002; Kochhann et al., 2017) and clumped isotope-based (Modestou et al., 2020) deep-ocean temperature reconstructions that suggest a temperature decrease of 1–3 °C (Fig. S4). Lear et al. (2010) Mg/Ca adjusted estimates describe temperatures of around 9.7–10 °C at 15 Ma and 8.2–8.5 °C at 13 Ma, implying a decrease of 1.2–1.8 °C across the transition at ODP Site 761. In that same study, for the unadjusted estimates, a decrease of 0.5–0.9 °C from ~8.5–8.6 °C at 15 Ma to 7.7–8 °C at 13 Ma is observed. Using data from the same site for clumped isotope analyses, Modestou et al. (2020) describe a decrease of 1.7 °C at ~15 Ma to 9.3 °C at ~12.9 Ma, or a decrease from an average of 11 °C during the 16.4–14.7 Ma interval (corresponding to the MMCO) to an average of 8.2 °C during the 12.9–11.8 Ma interval (corresponding to the post-MMCT), and thus a decrease of 2.9 °C between the two intervals. Our experiments show a decrease of 1.4 °C from 3.3 °C (MMCO400) to 1.9 °C (MMG200) for that site at 2000–2250 m depth.

For ODP Site 806, Lear et al. (2015) calculated a decrease of ~1.5 °C (1.2 °C), from ~8 °C (8 °C) at 15 Ma to ~6.5 °C (6.8 °C) after 13 Ma, using a linear (exponential) Mg/Ca-temperature calibration. However,

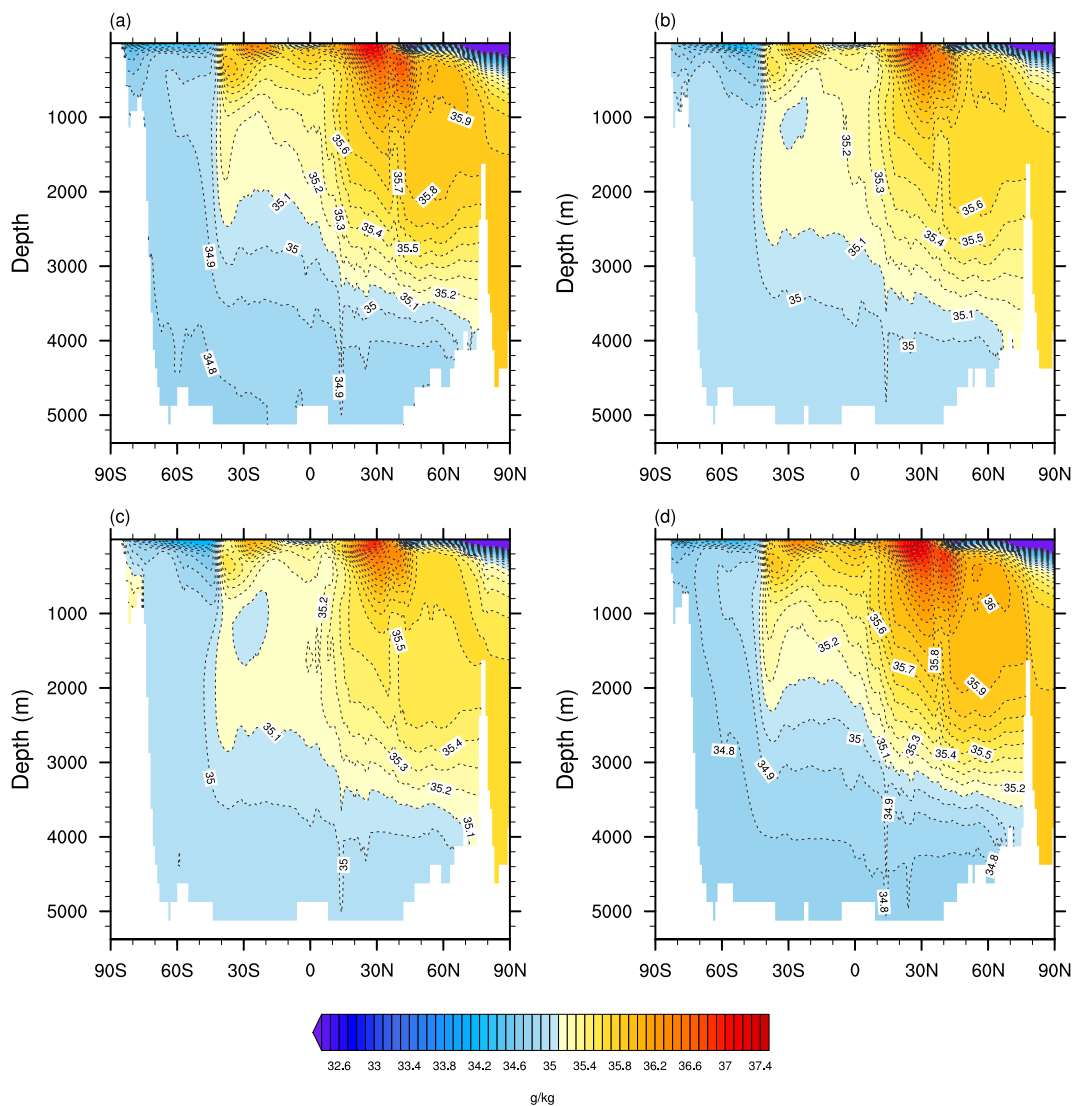


Fig. 10. Zonally averaged salinity for the Atlantic: a) MMCO400, b) MMG200, c) MMCO200, and d) MMG400, in g/kg. Note: Salinities are averaged over the longitude interval 100°W to 10°E.

that record shows high short-term variability, which makes it difficult to identify a time interval representative for the transition. Our values for that site at 2750–3000 m depth indicate a decrease of 1.7 °C from 2.5 °C (MMCO400) to 0.8 °C (MMG200). For ODP Site 747, [Billups and Schrag \(2002\)](#) Mg/Ca data indicate a decrease from 4.1 °C at 15.6 Ma to 3.13 °C at 12.9 Ma, thus ~ 1 °C decrease. In comparison, our model shows a decrease of ~ 2.3 °C from 2.9 °C at MMCO400 to 0.6 °C at MMG200 at 1500–1750 m depth (54.8°S, 78.51°E). At site 1171, the study by [Shevenell et al. \(2008\)](#) reports a decrease of ~ 2 °C from ~ 6 to 4 °C between 14.1 and 13.7 Ma of transient character, with subsequent warming of the same magnitude at 13.7–13.5 Ma. For that site, at 1500–1750 m depth, we modelled a drop of 2.0 °C from 3.6 °C to 1.6 °C, which is within the range of variability described in [Shevenell et al. \(2008\)](#). [Kochhann et al. \(2017\)](#) report cooling from ~ 5.2 °C to ~ 3.7 °C (a decrease of ~ 1.5 °C) between ~ 13.89 – 13.77 Ma for Site U1338 and from ~ 6.4 °C to ~ 5 °C (a decrease of ~ 1.4 °C) across approximately the same interval for Site 1146. A continuous temperature record spanning the whole MMCT is not available from that study. For Site U1338 we modelled a decrease of 1.9 °C, from 2.4 °C to 0.5 °C, and for Site 1146, of 1.63 °C, from 2.48 °C to 0.85 °C.

The CO₂ decrease causes significant cooling practically everywhere in the ocean, more pronounced in the upper cell of the MOC (associated

with cooling of NADW-equivalent water masses) compared to the lower cell. By contrast, the effect of the Antarctic ice-sheet expansion on ocean temperatures depends significantly on depth. While the upper ocean warms in response to ice-sheet growth, the deep ocean cools by about 0.5 °C associated with cooling of AABW equivalent water masses. This cooling adds to the CO₂-induced deep-ocean cooling of about 1–1.5 °C such that the total cooling of 1.5–2 °C is simulated. Even though the CO₂ cooling effect dominates over the Antarctic ice-sheet effect, the expansion of the ice-sheet contributes significantly to the deep-ocean temperature decline across the MMCT (about 25–30%). Model results by [Goldner et al. \(2014\)](#) show that the expansion of the Antarctic ice-sheet at the Eocene–Oligocene transition is fundamental in order to explain asymmetric cooling, enhanced in southern high latitudes and weaker in northern high latitudes and the subtropics, which models do not reproduce as a response to CO₂ alone. Similarly, in the current study, the Antarctic ice-sheet effect is key to explain the totality of the deep water cooling signal described in proxy records.

Since the Antarctic ice-sheet expansion has opposite effects on upper- and deep-ocean temperatures, the evolution of upper- and deep-ocean temperatures might have been partly asynchronous during the MMCT. We further surmise that the waxing and waning of the Antarctic ice-sheet through middle Miocene “glacial-interglacial” cycles had similar

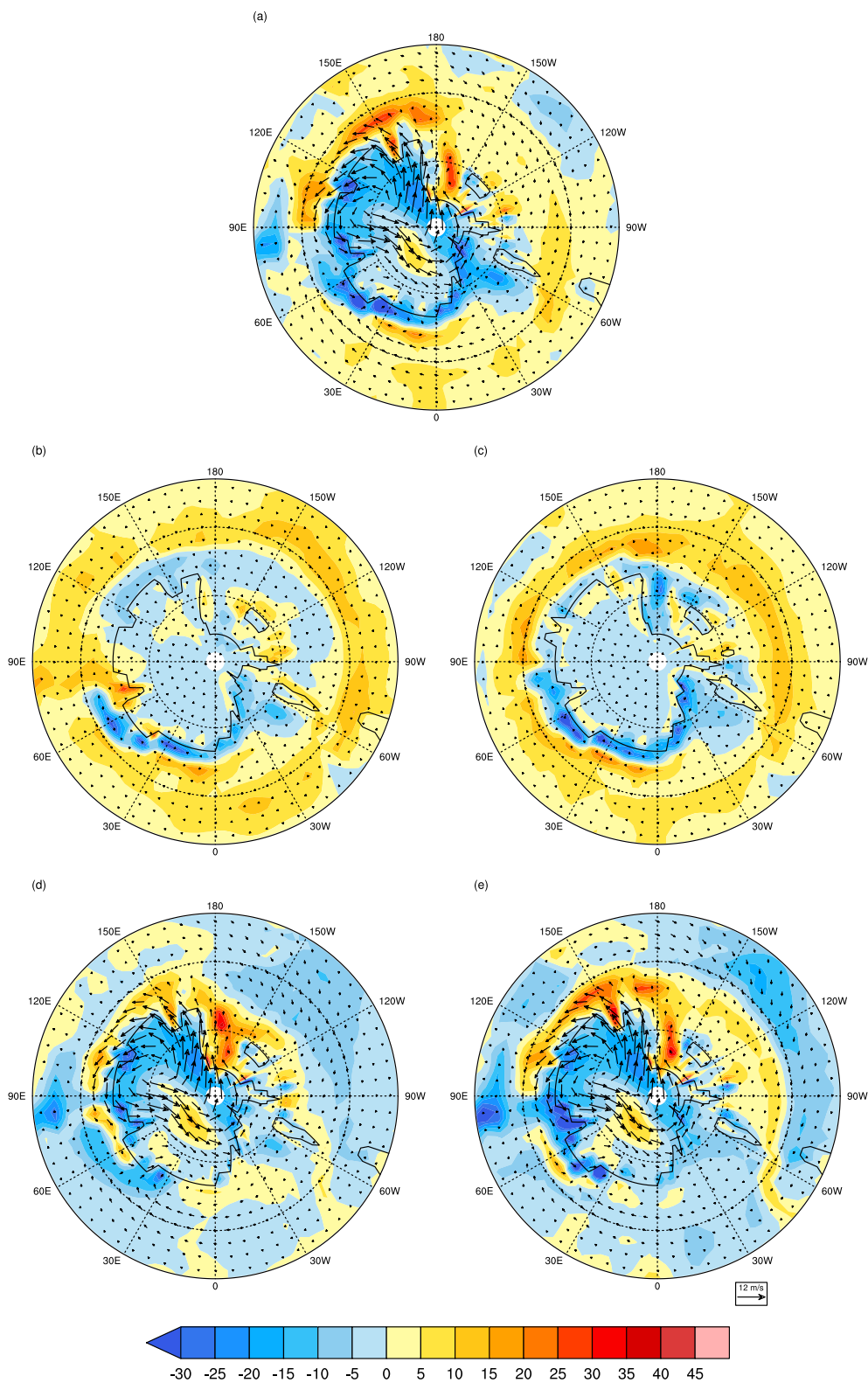


Fig. 11. Mean annual surface sensible heat-flux differences (positive is into the atmosphere), in W/m^2 , along with surface wind differences: a) MMG200-MMCO400 (MMCT), b) MMCO200-MMCO400 and c) MMG200-MMG400 (CO_2 effect), and d) MMG400-MMCO400 and e) MMG200-MMCO200 (ice-sheet effect). Latitude spans the interval 50–90°S.

effects on ocean temperatures at orbital time scales (cf. Passchier et al., 2013). These ~100 kyr cycles include variations in benthic $\delta^{18}O$ in the order of 1‰ (Holbourn et al., 2014; 2015). Our results suggest that BWT variations induced by glacial-interglacial changes in the Antarctic ice-sheet may explain a substantial portion of the observed $\delta^{18}O$ cycles.

As such, our model experiments may also provide insights into the middle Miocene glacial-interglacial climate variability addressed in the introduction.

In addition to deep-ocean cooling, the middle Miocene CO_2 drop also caused higher salinities and densities of the AABW equivalent waters

resulting in strengthening of the lower MOC cell. This finding is consistent with reconstructions of deep-ocean circulation, which suggest an increased production of southern-sourced deep and bottom water masses and hence improved deep-ocean ventilation after the MMCT (Flower and Kennett, 1995; Holbourn et al., 2013).

Convection of deep waters in the North Atlantic during the middle Miocene is a matter of debate (Kirillova et al., 2019). Von der Heydt and Dijkstra (2006) supported the existence of a North Atlantic cell already in the Late Oligocene and the Early Miocene. Hamon et al. (2013) described a well-defined North Atlantic cell during the middle Miocene. Our results describe a well-developed deep overturning cell in the North Atlantic during the middle Miocene, linked to the high salinity of Atlantic waters, in agreement with Von der Heydt and Dijkstra (2006) and Hamon et al. (2013). Additionally, our modelled MOC enhancement across the MMCT supports results by Huang et al. (2017) reporting weakening of oceanic poleward energy transport due to CO₂ increase as a response to meridional gradients of the CO₂ forcing.

In our Miocene simulations, sea ice is present in the Southern Ocean although less extensive than at PI. For the MMCO400 experiment, except for an ice-free region between 30°W and 50°E, our data indicate thicknesses of 0.5–1.0 m along the Antarctic coast (Fig. S7). Ice thicknesses above the mean are observed in the proto Ross and Weddell seas (1–3 m). Across the MMCT, sea ice increases significantly (~0.5–2 m) all along the Antarctic coast. The most outstanding increase (~4–7 m) occurs at 40–80°W, in the proto Weddell Sea. The MMCO400 simulation does not capture the ice-free or reduced sea ice conditions described for the Ross Sea during warm episodes in the middle Miocene (Levy et al., 2016).

In the Arctic Ocean, ice thicknesses of 0.5–1 m are modelled for the MMCO400, along with an increase of 0.5–1 m across the MMCT (Fig. S7). These values are significantly lower than the 6–7 m thicknesses PI values. Thus, according to the model, sea ice was present but thin during the middle Miocene in the Arctic. There is current controversy on Arctic ice cover during the Miocene, with some studies suggesting a perennial ice cover since at least 14 Ma (Darby, 2008) and other studies supporting the presence of seasonal ice during the colder late Miocene period (Stein et al., 2016). Our data would indicate a perennial though relatively thin ice cover.

In our experiments, the Tethys configuration was kept fixed, but there have been substantial changes in the Tethys region during the middle Miocene (Rögl, 1999). Its significance for the MMCT is a matter of debate in the literature (Flower and Kennett, 1994; Butzin et al., 2011; Hamon et al., 2013). Future studies should be aimed at further investigating how the Tethys configuration affects water masses, ocean circulation and heat transports. In particular, the role of Tethys waters as heat source in the Southern Ocean should be investigated with high-resolution models.

5. Conclusions

Our CCSM3 global analysis shows a middle Miocene climate warmer than PI, with mean global SSTs at MMCO400 and MMG200 about 2.8 °C and 1.2 °C higher than PI, respectively. Across the MMCT, modelled mean global SST cools by approximately 1.6 °C due to a decrease in atmospheric CO₂. In contrast, Antarctic ice-sheet expansion counteracts the global cooling with a slight warming effect on mean global SST due to decreased upwelling longwave flux over the elevated ice sheet. In general terms, proxy evidence suggests stronger cooling of surface waters across the MMCT compared to our values. Simulated deep-ocean temperatures decrease by 1.5–2 °C in most regions, in good agreement with proxy records. Most of this cooling is attributable to the atmospheric CO₂ decline, but for about 25–30% of the cooling, the expansion of the Antarctic ice-sheet is responsible by increasing cold air advection through wind strengthening. As a result, larger surface heat loss from the Southern Ocean produces colder AABW equivalent waters that spread northward. In addition, the salinity, density and formation rate of AABW

equivalent waters increase across the MMCT as indicated by a slightly stronger lower MOC cell. Our results further show evidence of a well-developed North Atlantic deep water overturning cell during the middle Miocene, which is linked to high salinities in the Atlantic basin.

Supplementary data to this article can be found online at <https://doi.org/10.1016/j.palaeo.2021.110591>.

Data availability

The experiment data used in this study are available on PANGAEA – Data Publisher for Earth & Environmental Science: <https://doi.pangaea.de/10.1594/PANGAEA.922944>.

Declaration of Competing Interest

The authors declare that they have no known competing financial interests or personal relationships that could have appeared to influence the work reported in this paper.

Acknowledgements

This study was part of the Marie Curie project “Throughflow”, funded by the EU 7th Framework Programme for Research, Technological Development and Demonstration [grant number 237922]. All model simulations were carried out on the Cray XC30/40 supercomputer of the Norddeutscher Verbund für Hoch- und Höchstleistungsrechnen (HLRN). An enormous thank you goes to Gabriel Gaus and Lars Nerger for their help in obtaining the model runs. We thank Catherine Bradshaw and an anonymous reviewer for their constructive comments that greatly improved the manuscript. We are especially grateful to Nan Rosenbloom (NCAR) for her help in the model setup, with further thanks going to Esther Brady, Gary Strand, Sam Levis, and Stephen Yeager. We would like to thank Thejna Tharammal, Ute Merkel, and Rima Rachmayani for their advice on the CCSM3 data analyses, as well as Andreas Manschke for the IT support. Finally, we would like to thank the graduate school GLOMAR and the “Throughflow” network for the useful courses and interdisciplinary exchange.

References

- Billups, K., Schrag, D.P., 2002. Paleotemperatures and ice volume of the past 27 Myr revisited with paired Mg/Ca and ¹⁸O/¹⁶O measurements on benthic foraminifera. *Paleoceanogr.* 17, 1003. <https://doi.org/10.1029/2000PA000567>.
- Burls, N.J., Bradshaw, C.D., De Boer, A.M., Herold, N., Huber, M., et al., 2021. Simulating Miocene warmth: insights from an opportunistic multi-model ensemble (MioMIP1). *Paleoceanogr. Palaeoclimatol.* 36, e2020PA004054 <https://doi.org/10.1029/2020PA004054>.
- Butzin, M., Lohmann, G., Bickert, T., 2011. Miocene Ocean circulation inferred from marine carbon cycle modeling combined with benthic isotope records. *Paleoceanography* 26, PA1203. <https://doi.org/10.1029/2009PA001901>.
- Collins, W.D., Bitz, C.M., Blackmon, M.L., Bonan, G.B., Bretherton, C.S., Carton, J.A., et al., 2006. The Community climate System Model Version 3 (CCSM3). *J. Clim.* 19, 2122–2143. <https://doi.org/10.1175/JCLI3761.1>.
- Cramer, B.S., Toggweiler, J.R., Wright, J.D., Katz, M.E., Miller, K.G., 2009. Ocean overturning since the late cretaceous: Inferences from a new benthic foraminiferal isotope compilation. *Paleoceanography* 24, PA4216. <https://doi.org/10.1029/2008PA001683>.
- Darby, D.A., 2008. Arctic perennial ice cover over the last 14 million years. *Paleoceanography* 23, PA1S07. <https://doi.org/10.1029/2007PA001479>.
- Flower, B.P., Kennett, J.P., 1993. Middle Miocene Ocean–climate transition: high resolution oxygen and carbon isotopic records from DSDP Site 588A, Southwest Pacific. *Paleoceanography* 8, 811–843.
- Flower, B.P., Kennett, J.P., 1994. The middle Miocene climatic transition: East Antarctic ice sheet development, deep ocean circulation and global carbon cycling. *Palaeogeogr. Palaeoclimatol. Palaeoecol.* 108, 537–555. [https://doi.org/10.1016/0031-0182\(94\)90251-8](https://doi.org/10.1016/0031-0182(94)90251-8).
- Flower, B.P., Kennett, J.P., 1995. Middle Miocene Deepwater paleoceanography in the Southwest Pacific: relations with East Antarctic Ice Sheet development. *Paleoceanography* 10, 1095–1112.
- Fretwell, P., Pritchard, H.D., Vaughan, D.G., Bamber, J.L., Barrand, N.E., Bell, R., Bianchi, C., et al., 2013. Bedmap2: improved ice bed, surface and thickness datasets for Antarctica. *Cryosphere* 7, 375–393. <https://doi.org/10.5194/tc-7-375-2013>.

- Frigola, A., Prange, M., Schulz, M., 2018. Boundary conditions for the Middle Miocene climate transition (MMCT v1.0). *Geosci. Model Dev.* 11, 1607–1626. <https://doi.org/10.5194/gmd-11-1607-2018>.
- Gasson, E., DeConto, R.M., Pollard, D., Levy, R.H., 2016. Dynamic Antarctic ice sheet during the early to mid-Miocene. *P. Natl. Acad. Sci. U. S. A.* 113, 3459–3464. <https://doi.org/10.1073/pnas.1516130113>.
- Goldner, A., Herold, N., Huber, M., 2014. Antarctic glaciation caused ocean circulation changes at the Eocene–Oligocene transition. *Nature* 511, 574–577. <https://doi.org/10.1038/nature13597>.
- Hall, R., 2012. Sundaland and Wallacea: Geology, plate tectonics and palaeogeography. In: Gower, D.J., et al. (Eds.), *Biotic Evolution and Environmental Change in Southeast Asia*. Cambridge University Press, Cambridge, U. K., pp. 32–78.
- Hamon, N., Sepulchre, P., Lefebvre, V., Ramstein, G., 2013. The role of eastern Tethys seaway closure in the Middle Miocene Climatic Transition (ca. 14 Ma). *Clim. Past* 9, 2687–2702. <https://doi.org/10.5194/cp-9-2687-2013>.
- Herold, N., Seton, M., Müller, R.D., You, Y., Huber, M., 2008. Middle Miocene tectonic boundary conditions for use in climate models. *Geochem. Geophys. Geosyst.* 9, Q10009 <https://doi.org/10.1029/2008GC002046>.
- Holbourn, A., Kuhnt, W., Simo, J.A.T., Li, Q., 2004. Middle Miocene isotope stratigraphy and paleoceanographic evolution of the northwest and southwest Australian margins (Wombat Plateau and Great Australian Bight). *Palaeogeogr. Palaeoclimatol. Palaeoecol.* 208, 1–22. <https://doi.org/10.1016/j.palaeo.2004.02.003>.
- Holbourn, A., Kuhnt, W., Schulz, M., Erlenkeuser, H., 2005. Impacts of orbital forcing and atmospheric carbon dioxide on Miocene ice-sheet expansion. *Nature* 438, 483–487. <https://doi.org/10.1038/nature04123>.
- Holbourn, A., Kuhnt, W., Schulz, M., Flores, J.A., Andersen, N., 2007. Orbitally-paced climate evolution during the middle Miocene “Monterey” carbon-isotope excursion. *Earth Planet. Sci. Lett.* 261, 534–550. <https://doi.org/10.1016/j.epsl.2007.07.026>.
- Holbourn, A., Kuhnt, W., Frank, M., Haley, B.A., 2013. Changes in Pacific Ocean circulation following the Miocene onset of permanent Antarctic ice cover. *Earth Planet. Sci. Lett.* 365, 38–50. <https://doi.org/10.1016/j.epsl.2013.01.020>.
- Holbourn, A., Kuhnt, W., Lyle, M., Schneider, L., Romero, O., Andersen, N., 2014. Middle Miocene climate cooling linked to intensification of eastern equatorial Pacific upwelling. *Geology* 42, 19–22. <https://doi.org/10.1130/G34890.1>.
- Holbourn, A., Kuhnt, W., Kochhann, K.G.D., Andersen, N., Meier, K.J.S., 2015. Global perturbation of the carbon cycle at the onset of the Miocene Climatic Optimum. *Geology* 43, 123–126. <https://doi.org/10.1130/G36317.1>.
- Huang, Y., Xia, Y., Tan, X., 2017. On the pattern of CO₂ radiative forcing and poleward energy transport. *J. Geophys. Res.-Atmos.* 122, 10,578–10,593. <https://doi.org/10.1002/2017JD027221>.
- John, C.M., Kamber, G.D., Browning, E., Leckie, R.M., Mateo, Z., Carson, B., Lowery, C., 2011. Timing and magnitude of Miocene eustasy derived from the mixed siliciclastic-carbonate stratigraphic record of the northeastern Australian margin. *Earth Planet. Sci. Lett.* 304, 455–467. <https://doi.org/10.1016/j.epsl.2011.02.013>.
- Kirilova, V., Osborne, A.H., Störling, T., Frank, M., 2019. Miocene restriction of the Pacific-North Atlantic throughflow strengthened Atlantic overturning circulation. *Nat. Commun.* 10, 4025. <https://doi.org/10.1038/s41467-019-12034-7>.
- Knorr, G., Lohmann, G., 2014. Climate warming during Antarctic ice sheet expansion at the Middle Miocene transition. *Nat. Geosci.* 7, 376–381. <https://doi.org/10.1038/ngeo2119>.
- Knorr, G., Butzin, M., Micheels, A., Lohmann, G., 2011. A warm Miocene climate at low atmospheric CO₂ levels. *Geophys. Res. Lett.* 38, L20701 <https://doi.org/10.1029/2011GL048873>.
- Kochhann, K.G.D., Holbourn, A., Kuhnt, W., Xu, J., 2017. Eastern equatorial Pacific benthic foraminiferal distribution and deep water temperature changes during the early to middle Miocene. *Mar. Micropaleontol.* 133, 28–39. <https://doi.org/10.1016/j.marmicro.2017.05.002>.
- Kominz, M.A., Browning, J.V., Miller, K.G., Sugarman, P.J., Mizintseva, S., Scotese, C.R., 2008. Late Cretaceous to Miocene sea-level estimates from the New Jersey and Delaware coastal plain cores: an error analysis. *Basin Res.* 20, 211–226. <https://doi.org/10.1111/j.1365-2117.2008.00354.x>.
- Kuhnert, H., Bickert, T., Paulsen, H., 2009. Southern Ocean frontal system changes precede Antarctic ice sheet growth during the middle Miocene. *Earth Planet. Sci. Lett.* 284, 630–638. <https://doi.org/10.1016/j.epsl.2009.05.030>.
- Langebroek, P.M., Paul, A., Schulz, M., 2009. Antarctic ice-sheet response to atmospheric CO₂ and insolation in the Middle Miocene. *Clim. Past* 5, 633–646. <https://doi.org/10.5194/cp-5-633-2009>.
- Langebroek, P.M., Paul, A., Schulz, M., 2010. Simulating the sea level imprint on marine oxygen isotope records during the middle Miocene using an ice sheet-climate model. *Paleoceanography* 25, PA4203. <https://doi.org/10.1029/2008PA001704>.
- Lear, C.H., Elderfield, H., Wilson, P.A., 2000. Cenozoic Deep-Sea Temperatures and Global Ice Volumes from Mg/Ca in Benthic Foraminiferal Calcite. *Science* 287, 269–272. <https://doi.org/10.1126/science.287.5451.269>.
- Lear, C.H., Mawbey, E.M., Rosenthal, Y., 2010. Cenozoic benthic foraminiferal Mg/Ca and Li/Ca records: toward unlocking temperatures and saturation states. *Paleoceanography* 25, PA4125. <https://doi.org/10.1029/2009PA001880>.
- Lear, C.H., Coxall, H.K., Foster, G.L., Lunt, D.J., Mawbey, E.M., Rosenthal, Y., Soudian, S.M., Thomas, E., Wilson, P.A., 2015. Neogene ice volume and ocean temperatures: insights from infaunal foraminiferal Mg/Ca paleothermometry. *Paleoceanogr. Paleoclimatol.* 30, 1437–1454. <https://doi.org/10.1002/2015PA002833>.
- Leutert, T.J., Auderset, A., Martínez-García, A., et al., 2020. Coupled Southern Ocean cooling and Antarctic ice sheet expansion during the middle Miocene. *Nat. Geosci.* 13, 634–639. <https://doi.org/10.1038/s41561-020-0623-0>.
- Levy, R., Harwood, D., Florindo, F., Sangiorgi, F., Tripathi, R., Von Eynatten, H., et al., 2016. Antarctic ice sheet sensitivity to atmospheric CO₂ variations in the early to mid-Miocene. *Proc. Natl. Acad. Sci. U. S. A.* 113, 3453–3458. <https://doi.org/10.1073/pnas.1516030113>.
- Modestou, S.E., Leutert, T.J., Fernandez, A., Lear, C.H., Meckler, A.N., 2020. Warm middle Miocene Indian Ocean bottom water temperatures: comparison of clumped isotope an Mg/Ca based estimates. *Paleoceanogr. Paleoclimatol.* <https://doi.org/10.1029/2020PA003927>.
- Montes, C., Cardona, A., McFadden, R., Moron, S.E., Silva, C.A., Restrepo-Moreno, S., et al., 2012. Evidence for middle Eocene and younger land emergence in Central Panama: Implications for Isthmus closure. *GSA Bull.* 124, 780–799. <https://doi.org/10.1130/B30528.1>.
- Morley, R.J., 2011. Cretaceous and Tertiary climate change and the past distribution of megathermal rainforests. In: Bush, M., Flenley, J., Gosling, W. (Eds.), *Tropical Rainforest Responses to Climatic Change*. Springer Praxis Books, Berlin, Heidelberg, pp. 1–34.
- Oerlemans, J., 2004. Correcting the Cenozoic δ₁₈O deep-sea temperature record for Antarctic ice volume. *Palaeogeogr. Palaeoclimatol.* 208, 195–205. <https://doi.org/10.1016/j.palaeo.2004.03.004>.
- Otto-Bliesner, B.L., Tomas, R., Brady, E.C., Ammann, C., Kothavala, Z., Clauzet, G., 2006. Climate sensitivity of moderate and low resolution versions of CCSM3 to preindustrial forcings. *J. Clim.* 19, 2567–2583. <https://doi.org/10.1175/JCLI3754.1>.
- Pälike, H., Lyle, M., Nishi, H., et al., 2012. A Cenozoic record of the equatorial Pacific carbonate compensation depth. *Nature* 488, 609–614. <https://doi.org/10.1038/nature11360>.
- Passchier, S., Falk, C.J., Florindo, F., 2013. Orbitally paced shifts in the particle size of Antarctic continental shelf sediments in response to ice dynamics during the Miocene climatic optimum. *Geosphere* 9, 54–62. <https://doi.org/10.1130/GES00840.1>.
- Pound, M.J., Haywood, A.M., Salzmann, U., Riding, J.B., 2012. Global vegetation dynamics and latitudinal temperature gradients during the Mid to late Miocene (15.97–5.33Ma). *Earth-Sci. Rev.* 112, 1–22. <https://doi.org/10.1016/j.earscirev.2012.02.005>.
- Raitzsch, M., Bijma, J., Bickert, T., Schulz, M., Holbourn, A., Kučera, M., 2021. Atmospheric carbon dioxide variations across the middle Miocene climate transition. *Clim. Past* 17, 703–719. <https://doi.org/10.5194/cp-17-703-2021>.
- Rögl, F., 1999. Mediterranean and Paratethys. Facts and hypotheses of an Oligocene to Miocene paleogeography (short overview). *Geol. Carpath.* 50, 339–349.
- Rousselle, G., Beltran, C., Sicre, M.-A., Raffi, I., De Rafélis, M., 2013. Changes in sea-surface conditions in the Equatorial Pacific during the middle Miocene–Pliocene as inferred from coccolith geochemistry. *Earth Planet. Sci. Lett.* 361, 412–421. <https://doi.org/10.1016/j.epsl.2012.11.003>.
- Sangiorgi, F., Bijl, P.K., Passchier, S., Salzmann, U., Schouten, S., McKay, R., Cody, R.D., Pross, J., van de Fliedert, T., Bohaty, S.M., Levy, R., Williams, T., Escutia, C., Brinkhuis, H., 2018. Southern Ocean warming and Wilkes Land ice sheet retreat during the mid-Miocene. *Nat. Commun.* 9, 317. <https://doi.org/10.1038/s41467-017-02609-7>.
- Shevenell, A.E., Kennett, J.P., Lea, D.W., 2004. Middle Miocene Southern Ocean Cooling and Antarctic Cryosphere expansion. *Science* 305, 1766–1770. <https://doi.org/10.1126/science.1100061>.
- Shevenell, A.E., Kennett, J.P., Lea, D.W., 2008. Middle Miocene ice sheet dynamics, deep-sea temperatures, and carbon cycling: a Southern Ocean perspective. *Geochem. Geophys. Geosyst.* 9, Q02006 <https://doi.org/10.1029/2007GC001736>.
- Singh, H.K.A., Bitz, C.M., Frierson, D.M.W., 2016. The global climate response to lowering surface orography of Antarctica and the importance of atmosphere–ocean coupling. *J. Clim.* 29, 4137–4153. <https://doi.org/10.1175/JCLI-D-15-0442.1>.
- Stein, R., Fahl, K., Schreck, M., et al., 2016. Evidence for ice-free summers in the late Miocene Central Arctic Ocean. *Nat. Commun.* 7, 11148. <https://doi.org/10.1038/ncomms11148>.
- Steinthorsdottir, M., Coxall, H.K., de Boer, A.M., Huber, M., Barbolini, N., Bradshaw, C.D., et al., 2021. The miocene: the future of the past. *Paleoceanogr. Paleoclimatol.* 36 (4), e2020PA004037 <https://doi.org/10.1029/2020PA004037>.
- Super, J.R., Thomas, E., Pagani, M., Huber, M., O’Brien, C., Hull, P.M., 2018. North Atlantic temperature and pCO₂ coupling in the early-middle Miocene. *Geology* 46 (6), 519–522. <https://doi.org/10.1130/G40228.1>.
- Super, J.R., Thomas, E., Pagani, M., Huber, M., O’Brien, C.L., Hull, P.M., 2020. Miocene evolution of the North Atlantic Sea surface temperature. *Paleoceanogr. Paleoclimatol.* 35, e2019PA003748 <https://doi.org/10.1029/2019PA003748>.
- Von der Heydt, A., Dijkstra, H.A., 2006. Effect of ocean gateways on the global ocean circulation in the late Oligocene and early Miocene. *Paleoceanography* 21, PA1011. <https://doi.org/10.1029/2005PA001149>.
- Wilson, D.S., Jamieson, S.S.R., Barrett, P.J., Leitchkov, G., Gohl, K., Larter, R.D., 2012. Antarctic topography at the Eocene–Oligocene boundary. *Palaeogeogr. Palaeoclimatol. Palaeoecol.* 335–336, 24–34. <https://doi.org/10.1016/j.palaeo.2011.05.028>.
- Wolfe, J.A., 1985. Distribution of major vegetational types during the Tertiary. In: Sundquist, E.T., Broecker, W.S. (Eds.), *The Carbon Cycle and Atmospheric CO₂: Natural Variations Archaean to Present*, Geophysical Monograph Series, 32. American Geophysical Union, Washington, D. C., pp. 357–375. <https://doi.org/10.1029/GM032p0357>.
- Woodruff, F., Savin, S., 1991. Mid-Miocene isotope stratigraphy in the deep sea: high resolution correlations, paleoclimatic cycles, and sediment preservation. *Paleoceanography* 6, 755–806. <https://doi.org/10.1029/91PA02561>.
- Zhang, Y.G., Pagani, M., Liu, Z., Bohaty, S.M., DeConto, R., 2013. A 40-million-year history of atmospheric CO₂. *Philos. T. Roy. Soc. A* 371, 20130096. <https://doi.org/10.1098/rsta.2013.0096>.